



# Microstructure and property of diamond-like carbon films with Al and Cr co-doping deposited using a hybrid beams system

Wei Dai<sup>a,\*</sup>, Jingmao Liu<sup>a</sup>, Dongsen Geng<sup>a</sup>, Peng Guo<sup>b</sup>, Jun Zheng<sup>c</sup>, Qimin Wang<sup>a,\*</sup>

<sup>a</sup> School of Electromechanical Engineering, Guangdong University of Technology, Guangzhou 510006, PR China

<sup>b</sup> Key Laboratory of Marine Materials and Related Technologies, Zhejiang Key Laboratory of Marine Materials and Protective Technologies, Ningbo Institute of Materials Technology and Engineering, Chinese Academy of Sciences, Ningbo 315201, PR China

<sup>c</sup> Science and Technology on Surface Engineering Laboratory, Lanzhou Institute of Physics, Lanzhou 730000, PR China



## ARTICLE INFO

### Article history:

Received 14 July 2015

Accepted 3 November 2015

Available online 5 November 2015

### Keywords:

Diamond-like carbon

Al:Cr co-doping

Residual stress

Elastic recovery

Tribology

## ABSTRACT

DLC films with weak carbide former Al and carbide former Cr co-doping (Al:Cr-DLC) were deposited by a hybrid beams system comprising an anode-layer linear ion beam source (LIS) and high power impulse magnetron sputtering using a gas mixture of  $C_2H_2$  and Ar as the precursor. The doped Al and Cr contents were controlled via adjusting the  $C_2H_2$  fraction in the gas mixture. The composition, microstructure, compressive stress, mechanical properties and tribological behaviors of the Al:Cr-DLC films were researched carefully using X-ray photoelectron spectroscopy, transmission electron microscopy, Raman spectroscopy, stress-tester, nanoindentation and ball-on-plate tribometer as function of the  $C_2H_2$  fraction. The results show that the Al and Cr contents in the films increased continuously as the  $C_2H_2$  fraction decreased. The doped Cr atoms preferred to bond with the carbon while the Al atoms mainly existed in metallic state. Structure modulation with alternate multilayer consisted of Al-poor DLC layer and Al-rich DLC layer was found in the films. Those periodic Al-rich DLC layers can effectively release the residual stress of the films. On the other hand, the formation of the carbide component due to Cr incorporation can help to increase the film hardness. Accordingly, the residual stress of the DLC films can be reduced without sacrificing the film hardness though co-doping Al and Cr atoms. Furthermore, it was found that the periodic Al-rich layer can greatly improve the elastic resilience of the DLC films and thus decreases the film friction coefficient and wear rate significantly. However, the existence of the carbide component would cause abrasive wear and thus deteriorate the wear performance of the films.

© 2015 Elsevier B.V. All rights reserved.

## 1. Introduction

Metal-containing diamond-like carbon (Me-DLC) films have attracted a great deal of research attention owing to their excellent mechanical, tribological and biological properties [1–3]. Furthermore, comparing to pure DLC films, Me-DLC films exhibit relatively low internal stress and high adhesion strength [4–6]. So far, numerous Me-DLC with doping different metal atoms have been deposited using various techniques. It was reported that the doped metal atoms could create a two-dimensional array of nano-clusters within the DLC matrix or an atomic-scale composite dissolving in the DLC matrix, and the chemical state and existence form of the doped metal atoms would pronouncedly influence the properties of the DLC films [7,8]. For instance, when the weak carbide former atoms, like Al [5] and Ag [6], were incorporated into DLC, they tended to form ductile metal phases without bonding with C. These

soft metallic phases imbedded in the carbon matrix can effectively improved toughness and released internal stress via the plastic deformation. However, the soft and ductile metal phases would also cause the film hardness to decrease. On the other hand, the carbide formers, like Ti [4] and W [9], would bond with C and form hard carbide phase in the carbon matrix when they were doped into the DLC. The hard composite can significantly improve the hardness of the films. Nevertheless, the formation of Me–C bond length would increase the disorder degree of the carbon matrix and thus cause the residual stress to increase. In addition, the increase of the hardness would limit the plasticity and decrease the toughness of the films. It is very difficult to acquire a DLC films with a combination property of high hardness and toughness, and low internal stress via doping one kind of weak carbon former metal atoms or carbide former metal atoms. Nevertheless, the co-doping of carbide former and weak-carbide former metal atoms has been expected to be a good way for improving the DLC films [10,11].

In this paper, DLC films with the co-incorporation of the weak carbide former Al and carbide former Cr (Al:Cr-DLC) were deposited using a hybrid beams source comprising an anode-layer linear

\* Corresponding authors.

E-mail addresses: [popdw@126.com](mailto:popdw@126.com) (W. Dai), [qmwang@gdut.edu.cn](mailto:qmwang@gdut.edu.cn) (Q. Wang).

ion beam source (LIS) and high power impulse magnetron sputtering (HIPIMS) which can significantly increase the ionization rate and energy of the species for the growth films as compared to the DC magnetron sputtering (DCMS) [12]. The composition, microstructure, internal stress, mechanical properties and tribological behaviors of the films were studied as a function of the  $C_2H_2$  fraction which was used to control the Al and Cr contents in the films. The relationships between the microstructure, internal stress, mechanical properties and tribological behaviors were discussed in detail.

## 2. Experimental details

Silicon (100) wafers of thickness at  $525 \pm 15 \mu m$  were used as the substrates, which were cleaned ultrasonically in acetone, ethanol, and dried in air before being put into the vacuum chamber. The Al:Cr-DLC films were prepared by the hybrid beams system which consists of the LIS and the HIPIMS equipped with a AlCr (Al/Cr = 70/30 at.%) revolving target (purity 99.99%). Prior to deposition, the substrates were sputter-cleaned for 20 min using Ar ions by the LIS at a bias voltage of  $-300 V$ . The base pressure was evacuated to the vacuum of  $3 \times 10^{-5} Pa$ . During depositing process, the pressure was kept at about  $0.5 Pa$ , and the substrate holder rotation speed was set at 4 rpm. A gas mixture of  $C_2H_2$  and Ar was introduced into the chamber as the gas precursor. The metal contents of Al and Cr in the films were controlled by varying the  $C_2H_2$  fraction in the precursor gases and the total gas flux (Ar and  $C_2H_2$ ) was kept at 100 sccm. Typical value of the LIS power was 1 kW (400 V and 2.5 A). For the HIPIMS unit, an average target power of 2 kW was maintained for all experiments. The target peak voltage was kept around 655 V. The pulse repetition frequency was 300 Hz and the pulse width was approximately 100  $\mu s$  (3% duty cycle). A bias voltage of  $-100 V$  was applied to the substrate. The whole deposition process-time was 2 h.

The thicknesses of the deposited films were measured by a cross-section SEM (Nova nanoSEM 430, FEI) measuring scale, and the film thicknesses are ranging from  $2.5 \mu m$  to  $3 \mu m$ . An X-ray photoelectron spectroscopy (XPS, Thermo ESCALAB 250Xi) with Al (mono) K $\alpha$  ( $h\nu = 1486.6 eV$ ) was used to characterize the chemical composition and chemical bonds of the deposited films. The XPS energy step size was 0.05 eV for the high-resolution spectrums. Before commencing the measurement,  $Ar^+$  ion beam was used to etch the sample surface for 5 min to remove contaminants. The contents of the elements in the films were calculated according to the atomic sensitivity factors and the relative area ratios of the peaks in XPS spectra of the films. And the hydrogen concentration in the films was neglected due to the lack of signal intensity in the current XPS detection measurement. High-resolution transmission electron microscopy of the films was performed on FEI Tecnai G2 F20S-Twin microscope with a 200 kV acceleration voltage. The TEM specimen were prepared by mechanical polishing and precision ion polishing system (Gatan PIPS691). The carbon atomic bond details of the films were characterized using Raman spectroscopy with incident light from a  $Ar^+$  laser at a wavelength of 514.5 nm.

Mechanical properties were measured by the nano-indentation technique with a indentation depth about 1/10th of the film thickness to minimize the substrate contribution. Six replicate indentations were made for each sample. The tribological behaviors of the films was measured using a ball-on-plate tribometer (Center for Tribology UMT-3) at room temperature with the humidity of 50% under dry sliding condition. A steel ball (GCr15, HRC60) with a diameter at 6 mm was used as the friction counter body. All the tests were performed at 20 mm/s sliding velocity for a sliding time of 1200 s and the applied load was 3 N. The length of the wear track was 5 mm and the reciprocating frequency was 2 Hz. After tests,

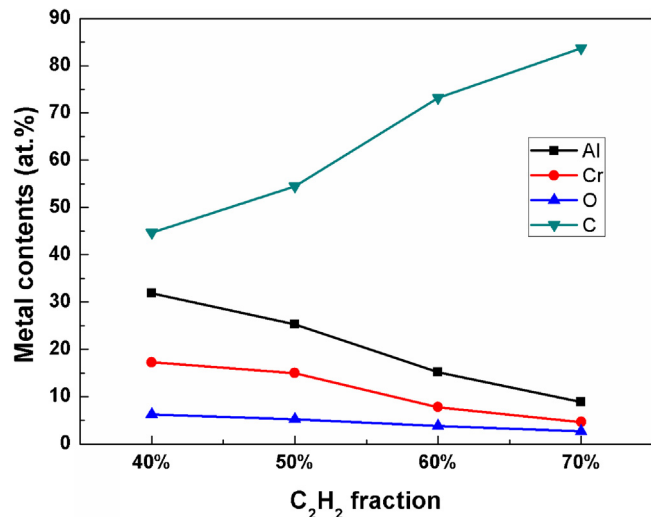


Fig. 1. Al, Cr, C and O contents of Al:Cr-DLC films as a function of the  $C_2H_2$  fraction in the gas mixture.

the wear track profiles were measured by the surface profilometer. And the wear rates were evaluated as volume per sliding distance per load.

## 3. Results and discussion

The evolution of the Al, Cr, C and O contents in the Al:Cr-DLC films is presented in Fig. 1 as a function of the  $C_2H_2$  fraction. It can be seen that as the  $C_2H_2$  fraction increased, both the Al and Cr contents decreased continuously from 31.8 at.% to 8.9 at.% and from 17.2 at.% to 4.7 at.%, respectively, while the C content increased from 44.7 at.% to 83.7 at.%, indicating that we can control the doped Al and Cr contents of the films via adjusting the  $C_2H_2$  fraction in gas mixture. The ratios of Cr and Ar in the films were kept at around 0.54, higher than that in the target ( $Cr/Al = 30/70$  at.%) we used. This phenomenon might be due to the higher sputtering rate of Cr than that of Al. A small amount of oxygen (not higher than 5 at.%) was found in the films. The existence of oxygen can be mainly attributed to the residual oxygen in the chamber due to the relatively high base pressure.

High resolution XPS spectra for the Al2p, Cr2p, and C1s regions of the films are plotted in Fig. 2(a)–(c), respectively. It can be seen that the intensities of the Al2p and Cr2p peaks increased with decreasing  $C_2H_2$  fraction, indicating that the Al and Cr contents increased. The Al2p spectra could be deconvoluted into two peaks: a major peak around 73 eV and a weak peak around 75 eV, corresponding to Al in the metallic state and Al in oxide state, respectively. This result indicates that aluminum did not bond with carbon to form carbide, which can also be illustrated by the C1s spectra. Normally, aluminum carbide has a binding energy at 281.5 eV and aluminum oxycarbide has a binding energy at 282.5 eV [13,14]. However, both of them were not observed in the C1s spectra of the films, as shown in Fig. 2(c). The Cr2p spectra reveal a symmetrical sharp peak centered at  $\sim 574 eV$ , as expected for the  $2p_{3/2}$  state of the metallic Cr. A small peak at  $\sim 575 eV$  deconvoluted from the major peak could be assigned to Cr–O bonds. However, there is no significant difference between the Cr2p peaks in those Al:Cr-DLC films. Previous paper indicated that the Cr2p peak could not be used effectively to differentiate the chemical bonds between metallic Cr and Cr carbide [7]. Nevertheless, the C1s spectrum can be used to determine the existence of the carbide. The C1s spectra of the films could be fitted with three peaks. The peak at the relatively lower binding energy of about 283 eV could be assigned to Cr–C bonding and the

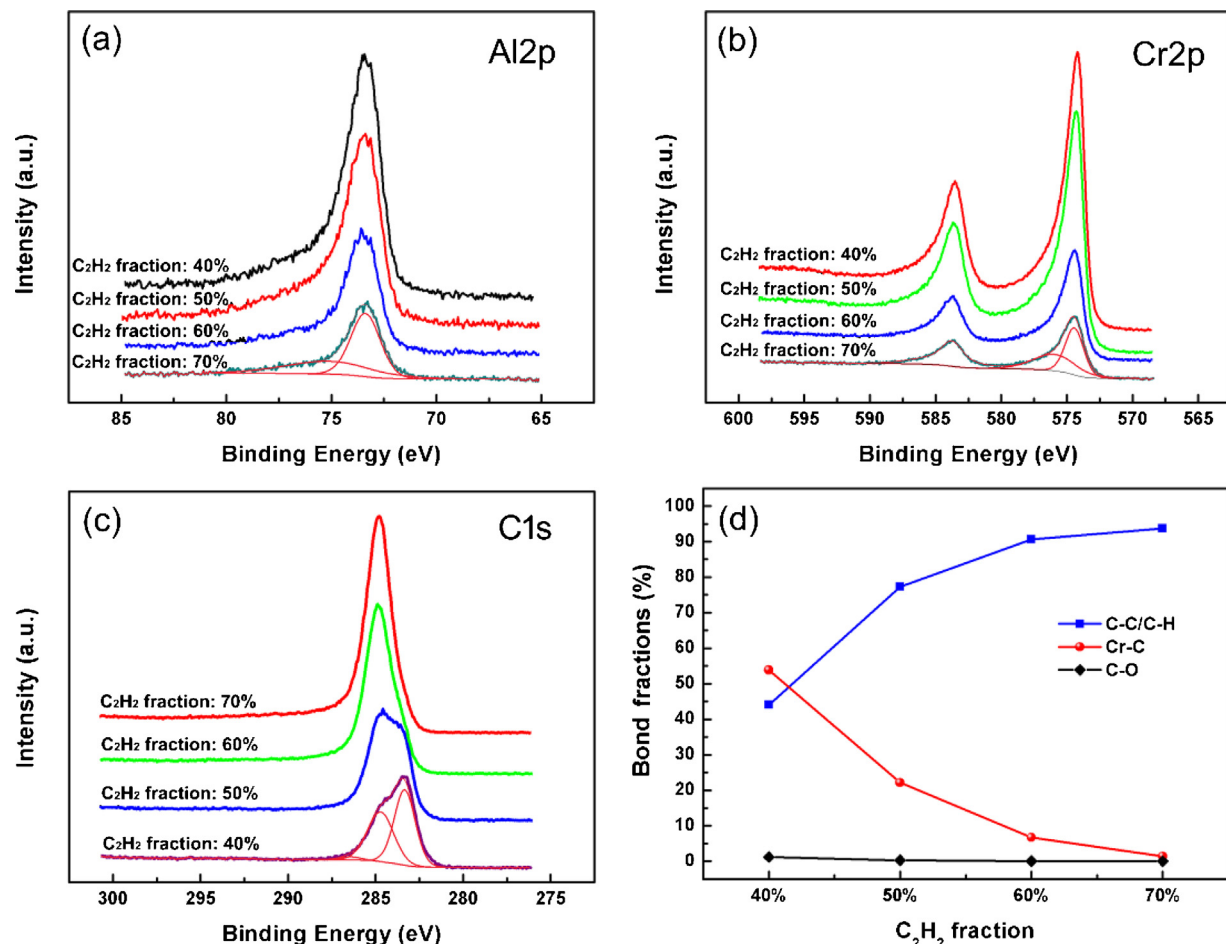


**Fig. 2.** High resolution XPS spectra for (a) Al2p; (b) Cr2p; and (c) C1s regions for the films; (d) the bonding fractions of the Cr—C, C—C/C—H and C—O bonds in films were determined by the relative peak areas of the fitted peaks of the C1s spectra in Fig. 2(c).

peak around 285 eV was expected to originate from the typical C—C or C—H bonding in DLC films. A weak peak appears at the binding energy of about 286 eV corresponding to C—O bonds. It should be noted that a shift of the major peak of the C1s spectra from the carbide bonding energy to higher C—C or C—H bonding energy was observed, as the  $C_2H_2$  fraction increased from 40% to 70%, implying that the film structure transformed from a carbide feature to an amorphous carbon feature.

The bond fractions of the Cr—C (carbide phase), C—C/C—H (DLC phase) and C—O bonds in films were determined by the relative peak areas of the fitted peaks of the C1s spectra and are presented in Fig. 2(d). The C—O bond in the films had remained fairly constant with a value lower than 1% since the residual O favored to bond with Al and Cr rather than C. Initially, the carbide bond fraction was about 53.8%, higher than the C—C/C—H bond fraction of about 44%. This means that the film deposited at the  $C_2H_2$  fraction of 30% was dominantly consisted of carbide phase. As the  $C_2H_2$  fraction increased, the carbide bond fraction decreased continuously while the C—C/C—H fraction changed in the opposite trend simultaneously. When the  $C_2H_2$  fraction reached to 70%, the carbide bond fraction decreased to 1.4% and the C—C/C—H bond fraction increased to 93.8%, indicating that the film was dominantly consisted of DLC phase.

Many papers reported that the carbide structures could be formed just as the content of the doped metal atom exceeded its solid solubility limit in the DLC matrix, which was significantly correlated with the nature of the doped metal as well as the deposition technique [7,15–17]. It is noteworthy that Cr—C was still found in

the as-deposited films when the Cr content was as low as 4.7 at.%, which means that the Cr atoms in the films had a solid solubility limit of <4.7 at.%. This value is much lower than the solid solubility limit (about 8.42 at.%) of the Cr atoms in the DLC films deposited by a similar hybrid ion beam system consisted of the LIS and DCMS in our previous paper [18]. The decrease of the solid solubility may be related to the replacement of the DCMS with the HIPIMS. It is well established that the HIPIMS plasma is characterized by a more intense energetic ion bombardment as compared to DCMS, which can facilitate the chemical reactions of the carbon and doped metal atoms [19,20]. In addition, the co-incorporation of Al may also had some effect on the solid solubility limit of the Cr in the DLC matrix through occupying the interspaces of the carbon matrix.

The carbon structure of the films was characterized using Raman spectroscopy, which is a popular and effective tool to characterize the carbon bonding in DLC films. The Raman spectra of the Al:Cr-DLC films deposited at different  $C_2H_2$  fractions are shown in Fig. 3(a). There is a broad asymmetric Raman scattering band in the range of 1000–1700 cm<sup>-1</sup>, representing the typical characteristic of DLC film [21]. Normally, the asymmetric Raman spectra of DLC films can be fitted using two Gaussian peaks: the G-peak around 1580 cm<sup>-1</sup> and the D-peak around 1360 cm<sup>-1</sup>, as shown in Fig. 3(a). The G peak is due to the vibrations of C—C stretching of all pairs of sp<sup>2</sup> atoms in both aromatic rings and carbon chains, and the D peak is due to symmetric breathing vibration of sp<sup>2</sup> atoms only in rings [22,23]. According to the G-peak position and the intensity ratio of D-peak to G-peak ( $I_D/I_G$ ), the sp<sup>2</sup>/sp<sup>3</sup> ratios of the DLC films can be characterized. In hydrogenated amorphous carbon, an decrease in

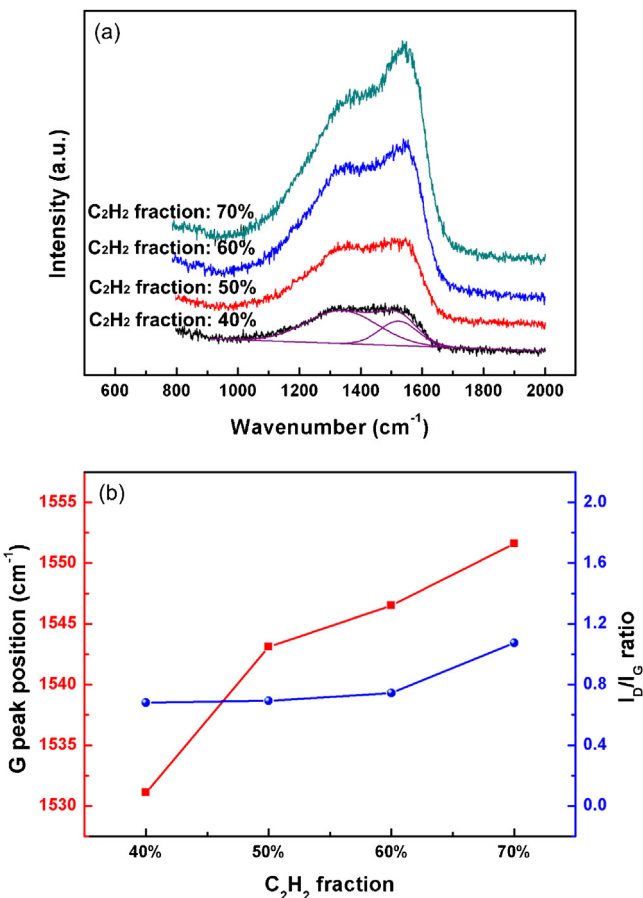


**Fig. 3.** (a) Raman spectra of the Al:Cr-DLC films deposited at different C<sub>2</sub>H<sub>2</sub> fractions; and (b) The corresponding G peak position and the  $I_D/I_G$  ratio of the films as a function of Cu concentration.

the G peak toward lower wavenumber and the  $I_D/I_G$  ratio correspond to an decrease in  $sp^2/sp^3$  ratio [21–23]. The corresponding G peak position and the  $I_D/I_G$  ratio of the films, after fitted, are clarified in Fig. 3(b). As the C<sub>2</sub>H<sub>2</sub> fraction increased (the contents of the doped Al:Cr atoms decreased), the G peak position shifted toward high wavenumber and the  $I_D/I_G$  ratio increased, indicating that the  $sp^2/sp^3$  ratio decreased with the doped Al and Cr contents. This phenomenon may be related to the relative lower bonding energy of  $sp^2$ -C than that of  $sp^3$ -C, which made  $sp^2$ -C favorable to bond with the Cr atoms to form the Cr–C bond. As a result, a larger number of  $sp^2$ -C were consumed in formation of carbide and thus resulted in the decrease of  $sp^2/sp^3$  ratio. Additionally, since that the carbide bonding length was longer than the C–C bond, the presence of Cr–C bonds would cause an increase of the disorder degree that is linked to higher  $sp^3$  content in DLC [22].

To obtain insight into the microstructure of Al:Cr-DLC films, the typical TEM micrographs of the film deposited at the C<sub>2</sub>H<sub>2</sub> fraction of 60% are presented Fig. 4. It can be seen that the film shows a periodically layered structure, as shown in Fig. 4(a). The total periodicity of the layers ranges from 6 to 8 nm. A line-scan EDX compositional measurement crossing the periodical layers (noted by the red arrow in Fig. 4(a)) was made to identify the variation of the film composition, as shown in Fig. 4(d). It was found that the elements of Al, Cr and C also showed periodical variations in EDX intensity, and the intensity of Al reached the peak value at white layers while the C amount was small. So, we believed that the periodical multilayered structure was consisted of the Al-rich layer (white layer) and Al-poor layer (dark layer). The formation of the periodical multilayered structure might be related with the

rotation of the substrate holder which faced to the LIS and AlCr target in turn. It should be noted that numerous isolated globular grains were observed in the magnified view of Fig. 4(b). We believed that these globular grains were the carbide nano-clusters. However, these carbide nano-clusters have very small sizes of approximately 2 nm in diameter. This may be attributed to the low content of the doped Cr (7.8 at.%) at the C<sub>2</sub>H<sub>2</sub> fraction of 60%. The diffraction ring of the corresponding SAED (Fig. 4(c)) also indicated the existence of the carbide phase, although the diffraction rings is not so clear due to the small sizes of the carbide nano-clusters.

Fig. 5 reveals the variation of residual stress of the films as a function of the C<sub>2</sub>H<sub>2</sub> fraction. The residual stress of the films decreased as the C<sub>2</sub>H<sub>2</sub> fraction decreased, indicating that the incorporation of metal atoms can significantly decrease the film residual stress. The residual stress of DLC is expected to arise from the formation process of  $sp^3$ -C and therefore is proportional to the  $sp^3$ -C content (disorder degree) of the DLC films [21]. According to the Raman results above, the incorporation of Cr atoms would cause an increase of the disorder degree as well as  $sp^3$  content of the films due to the formation of Cr–C bonds, and thus should increase the residual stress of the films, as reported in other papers where the formation of carbide bonds would also cause the film residual stress to increase [4,9,24]. In the present paper, conversely, the residual stress decreased as the C<sub>2</sub>H<sub>2</sub> fraction decreased (According to the XPS results above, the decrease of the C<sub>2</sub>H<sub>2</sub> fraction resulted in high fraction of Cr–C bonds in the films). It is clear that the continuous declination of the film residual stress regarding to the Cr–C fraction was related to the incorporation of Al. Some people believed that the reduction of residual stress was attributed to the increase of  $sp^2$  fraction in films caused by the incorporation of Al [25,11]. Unfortunately, the  $sp^3$ -C fraction of the films increased with the doped Al and Cr contents in this paper. Accordingly, we thought that the relaxation of stress could be realized via the plastic deformation of these Al-rich multilayered structure rather than the increase of  $sp^2$  fraction.

The hardness  $H$  and elastic modulus  $E$  of the films deposited at various C<sub>2</sub>H<sub>2</sub> fractions are presented in Fig. 6(a). It can be seen that the films changed very little on the hardness with the C<sub>2</sub>H<sub>2</sub> fraction, except the film deposited at the C<sub>2</sub>H<sub>2</sub> fraction of 40% which showed a relatively high hardness. Usually, the mechanical properties of DLC films mainly depend on the  $sp^3$  carbon interlink matrix [21]. The Raman results show that the  $sp^3$ -C fraction increased as the C<sub>2</sub>H<sub>2</sub> fraction decreased (the doped Al and Cr contents increased), which would contribute to the increase of the film hardness. In addition, the hard carbide phase formed in the films would also increased the film hardness. So the film deposited at the C<sub>2</sub>H<sub>2</sub> fraction of 40% exhibited the highest hardness. This result implies that we can effectively decrease the residual stress of the DLC films without sacrificing the film hardness though co-doping Al and Cr atoms. On the other hand, it is characteristic to note that the elastic modulus decreased continuously with the C<sub>2</sub>H<sub>2</sub> fraction, which means that we can tune the hardness-elastic modulus ratios ( $H/E$ ) of the films via adjusting the C<sub>2</sub>H<sub>2</sub> fraction (the doped Al and Cr contents). The  $H/E$  ratio is expected to correlate with the elastic resilience and a high  $H/E$  ratio is related to a high elastic strain prior to the plastic deformation [26].

The  $H/E$  ratios of the films are presented in Fig. 6(b). It can be seen the  $H/E$  ratio of the film increased with the C<sub>2</sub>H<sub>2</sub> fraction and a maximum value of approximately 0.1 was acquired at 70%, indicating that the film deposited at 70% C<sub>2</sub>H<sub>2</sub> fraction had the highest elastic resilience among these films. As the C<sub>2</sub>H<sub>2</sub> fraction decreased (the doped Al and Cr contents increased), a mass of brittle carbide phase was formed in the films, which would cause the  $H/E$  ratio of the film to decrease. The elastic resilience of the films can also be estimated through the nano-indentation load-displacement curves of the films, where the elastic recovery  $R$  can be defined as the ratio

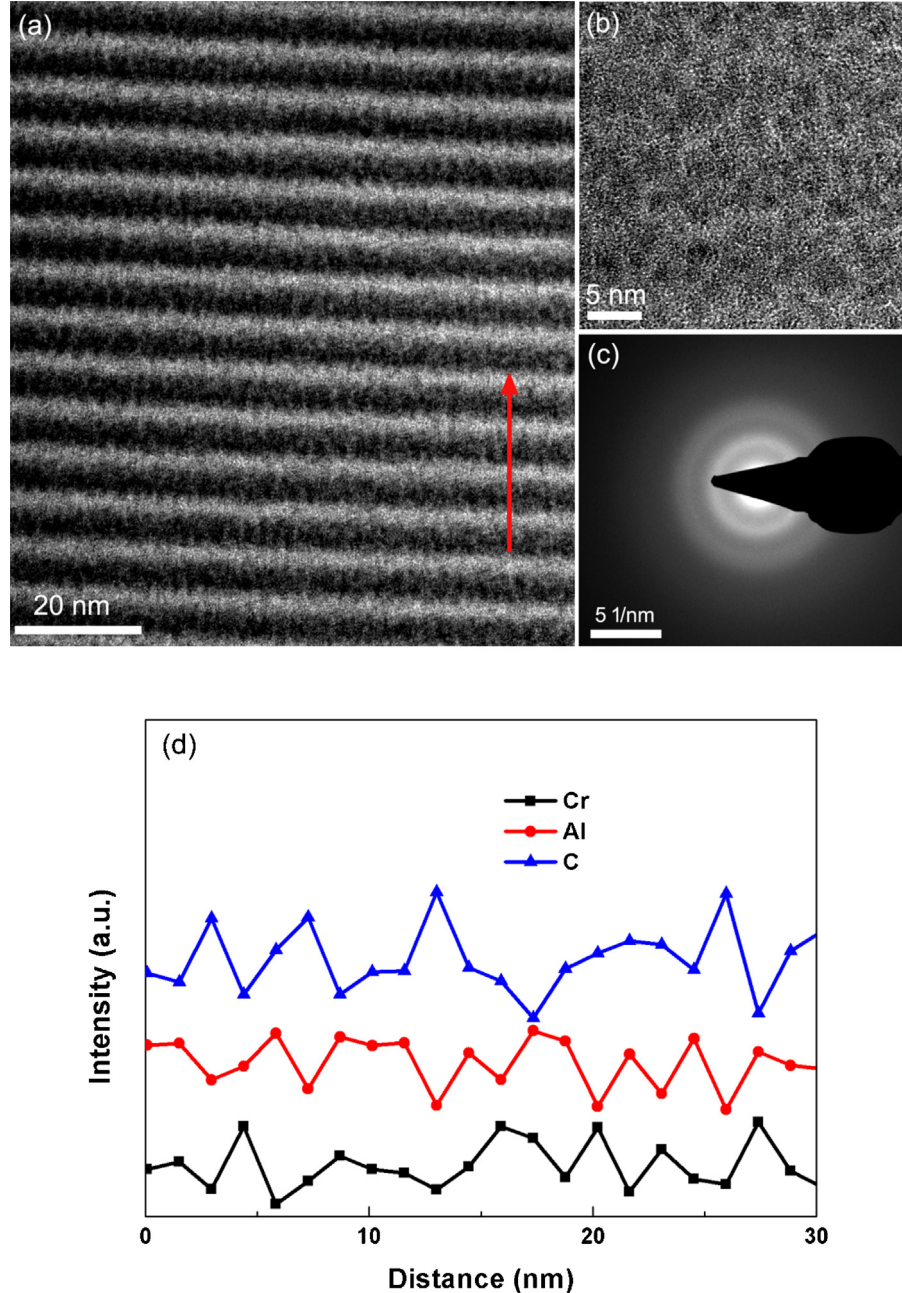


**Fig. 4.** (a) TEM micrograph; (b) the corresponding high magnification micrograph; and (c) the corresponding SAED pattern of the film deposited at the  $\text{C}_2\text{H}_2$  fraction of 60%; (d) linescan EDX compositional measurement along the arrow in Fig. 4(a).

of the part of the indentation depth that can be recovered (i.e., the elastic depth) to the maximum indentation depth [27]. It can be seen that the variation of the elastic recovery  $R$  showed in Fig. 6(b) is similar to the  $H/E$  ratio. It is also worthy to note that all the Al:Cr-DLC films exhibited a recovery  $R$  of >50%, which is much higher than the pure DLC films of about 39% [28]. The improvement of the elastic resilience of the films might be mainly attributed to the formation of the ductile Al-rich multilayered structures in the carbon matrix as shown in the TEM image. These ductile metal structures have been expected to overcome the brittleness and improve the toughness of the DLC films [11,29]. The high  $H/E$  ratio and elastic recovery  $R$  are very conducive to tribological properties of the films [30].

The tribological tests of the deposited Al:Cr-DLC films were performed on the ball-on-plate tribometer. The friction coefficient of the films as a function of sliding duration was shown in Fig. 7(a),

and the average friction coefficients and wear rate regarding to the  $\text{C}_2\text{H}_2$  fraction were presented in Fig. 7(b). It can be seen that the films deposited at the  $\text{C}_2\text{H}_2$  fraction of 70% exhibited a relatively steady and low friction coefficient lower than 0.12, and a very small wear rates of about  $1.7 \times 10^{-15} \text{ mm}^3 \text{ N}^{-1} \text{ m}^{-1}$ . As the  $\text{C}_2\text{H}_2$  fraction decreased, the friction coefficient and wear rate of the films increased. Specially for the  $\text{C}_2\text{H}_2$  fraction of 40%, although the film has the highest hardness at this point, the friction coefficient and wear rate reached to the highest values of about 0.25 and  $2.1 \times 10^{-13} \text{ mm}^3 \text{ N}^{-1} \text{ m}^{-1}$ , respectively. At a relatively high the  $\text{C}_2\text{H}_2$  fraction (i.e. 70%), the films possess a high  $H/E$  ratio and elastic recovery  $R$ , which are believed to effectively reduce the contact pressure of the friction pairs via distributing the applied load over a larger area [31]. As a result, the films displayed excellent tribological properties with a low friction coefficient and wear rate.

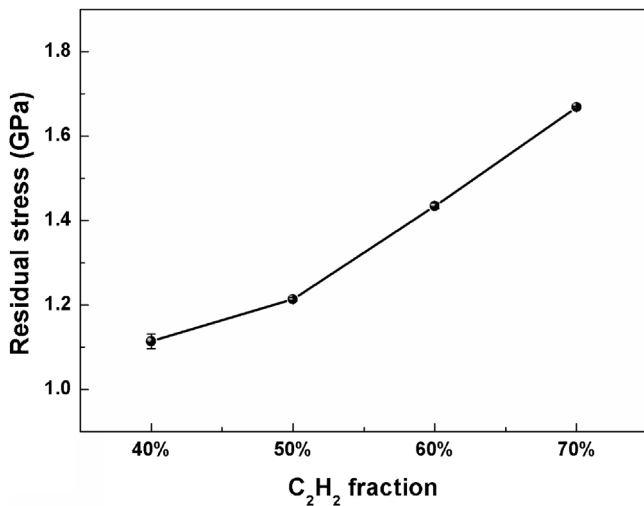


Fig. 5. Residual stress of the Al:Cr-DLC films as a function of the  $C_2H_2$  fraction.

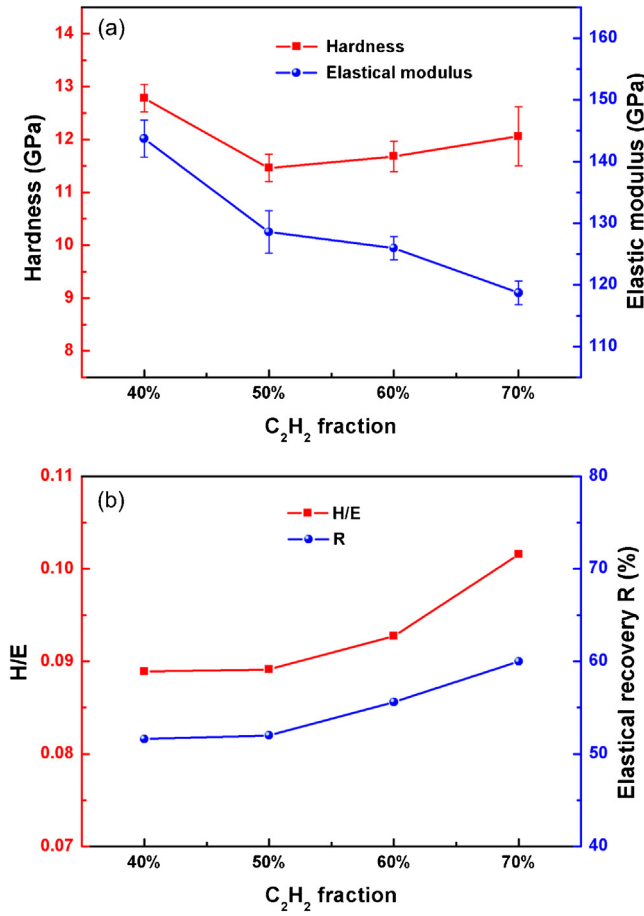


Fig. 6. (a) Hardness and elastic modulus of the films as a function of the  $C_2H_2$  fraction; and (b) the hardness-modulus ratios and elastic recovery  $R$  of the films deposited at different  $C_2H_2$  fractions. The  $R$  was defined as the ratio of the part of the indentation depth that can be recovery to the maximum indentation depth in nano-indentation load-displacement curves.

However, as the  $C_2H_2$  fraction decreased, the  $H/E$  ratio and elastic recovery  $R$  of the films decreased, which caused the contact pressure and wear to increase. In addition, as the doped Cr contents increased, a large amount of hard carbide phase was formed in the DLC matrix and the film was gradually transformed into a

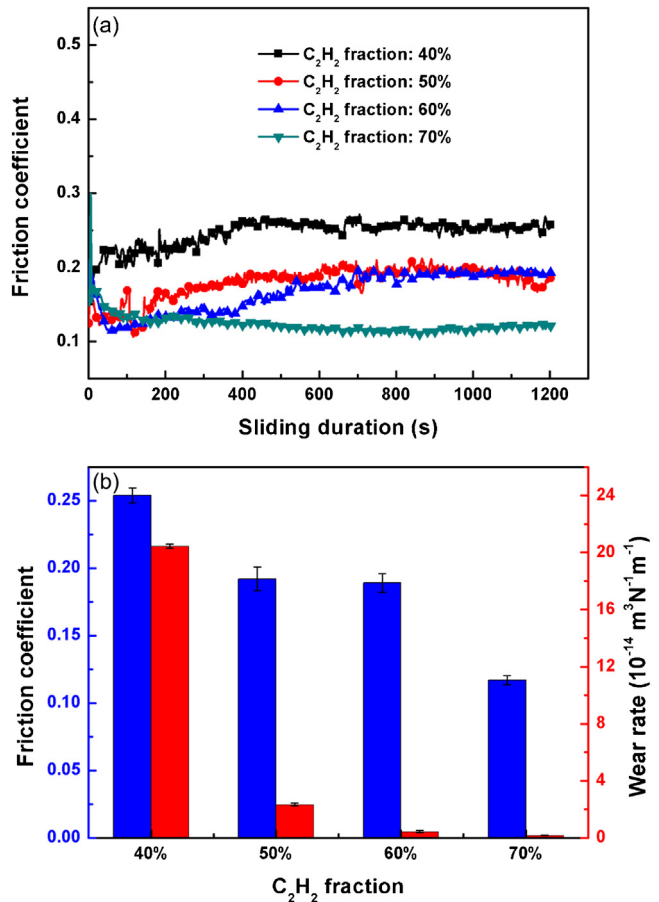


Fig. 7. (a) The friction coefficient of the films as a function of sliding duration; and (b) the average friction coefficients and wear rate regarding to the  $C_2H_2$  fraction.

carbide-rich film. This would cause abrasive wear and thus deteriorate the wear performance, as verified by the obtained high friction coefficient and wear rate.

#### 4. Conclusions

Al:Cr-DLC films were deposited using the hybrid ion beam system composed of the LIS and the HIPIMS with the AlCr target ( $Al/Cr = 70/30$  at.%). The doped Al and Cr contents in the films ranged from 8.9 at.% to 31.8 at.% and from 4.7 at.% to 17.2 at.%, respectively, via adjusting the  $C_2H_2$  fraction from 70% to 40% in gas mixture of  $C_2H_2$  and Ar. The carbide former Cr doped into DLC matrix preferred to bond with C to form carbide components which could be conducive to improving the hardness of the films, while the weak carbide former Al existed in metallic state and presented as Al-rich multilayered structure. The residual stress of the films can be significantly released by the formation of these Al-rich layers. In addition, the Al-rich layer was expected to improve the film elastic recovery which were proposed as a key parameter in wear. As a result, the film with the maximum elastic recovery deposited at  $C_2H_2$  fraction of 70% exhibited an excellent tribological performance with very low friction coefficient (0.12) and wear rate ( $1.7 \times 10^{-15} \text{ mm}^3 \text{ N}^{-1} \text{ m}^{-1}$ ). However, the formation of the hard carbide in the DLC matrix would cause abrasive wear and thus deteriorate the wear performance, resulting in high friction coefficient and wear rate.

## Acknowledgments

This work was financially supported in part by the projects of the National Natural Science Foundation of China (Grant No: 51405088) and the National Natural Science Foundation of Guangdong province (Grant No: 2014A030313516). It was also supported in part by a grant from the Zhujiang New Star of Science and Technology of Guangzhou City (Grant No: 201506010091).

## References

- [1] K. Bewilogua, D. Hofmann, *Surf. Coat. Technol.* 242 (2014) 214.
- [2] C.A. Love, R.B. Cook, T.J. Harvey, P.A. Dearnley, R.J.K. Wood, *Tribol. Int.* 63 (2013) 141.
- [3] R. Hauert, *Diamond Relat. Mater.* 12 (2013) 583.
- [4] J. Cui, L. Qiang, B. Zhang, X. Ling, T. Yang, J. Zhang, *Appl. Surf. Sci.* 258 (2012) 5025.
- [5] W. Dai, A. Wang, *J. Alloys Compd.* 509 (2011) 4626.
- [6] N.K. Manninen, F. Ribeiro, A. Escudeiro, T. Polcar, S. Carvalho, A. Cavaleiro, *Surf. Coat. Technol.* 232 (2013) 440.
- [7] V. Singh, J.C. Jiang, E.I. Meletis, *Thin Solid Films* 189 (2005) 150.
- [8] P. VijaiBharathy, D. Nataraj, P.K. Chu, H. Wang, Q. Yang, M.S.R.N. Kiran, J. Silvestre-Albero, D. Mangalaraj, *Appl. Surf. Sci.* 257 (2010) 143.
- [9] A.Y. Wang, K.R. Lee, J.P. Ahn, J.H. Han, *Carbon* 44 (2006) 1826.
- [10] S. Zhou, L. Wang, Q. Xue, *Diamond Relat. Mater.* 21 (2012) 58.
- [11] S. Zhang, X.L. Bui, Y. Fu, *Thin Solid Films* 467 (2004) 261.
- [12] J.T. Gudmundsson, J. Alami, U. Helmersson, *Surf. Coat. Technol.* 161 (2002) 249.
- [13] B. Maruyama, F.S. Ohuchi, L. Rabenberg, *Mater. Sci. Lett.* 9 (1990) 864.
- [14] G. Zhang, P. Yan, P. Wang, Y. Chen, J. Zhang, *J. Phys. D: Appl. Phys.* 40 (2007) 6748.
- [15] X. Fan, E.C. Dickey, S.J. Pennycook, M.K. Sunkara, *Appl. Phys. Lett.* 75 (1999) 2740.
- [16] W.J. Meng, R.C. Tittsworth, L.E. Rehn, *Thin Solid Films* 377–378 (2000) 222.
- [17] C.H. Liang, W.L. Wang, C.F. Huang, H.Y. Tsai, C.C. Yang, *Ceram. Int.* 40 (2014) 13329.
- [18] W. Dai, P. Ke, A. Wang, *Vacuum* 85 (2011) 792.
- [19] V. Kouznetsov, K. Macak, J.M. Schneider, U. Helmersson, I. Petrov, *Surf. Coat. Technol.* 122 (1999) 290.
- [20] M. Samuelsson, K. Sarakinos, H. Hogberg, E. Lewin, U. Jansson, B. Walivaara, H. Ljungcrantz, U. Helmersson, *Surf. Coat. Technol.* 206 (2012) 2396.
- [21] J. Robertson, *Mater. Sci. Eng. R* 37 (2002) 129.
- [22] C. Casiraghi, A.C. Ferrari, J. Robertson, *Phys. Rev. B* 72 (2005) 085401.
- [23] N. Dwivedi, E. Rismani-Yazdi, R.J. Yeo, P.S. Goohpattader, N. Satyanarayana, N. Srinivasan, B. Druz, S. Tripathy, C.S. Bhatia, *Sci. Rep.* 4 (2014) 5021.
- [24] L. Ji, H. Li, F. Zhao, J. Chen, H. Zhou, *Diamond Relat. Mater.* 17 (2008) 1949.
- [25] B.K. Tay, Y.H. Cheng, X.Z. Ding, S.P. Lau, X. Shi, G.F. You, D. Sheeja, *Diamond Relat. Mater.* 10 (2001) 1082.
- [26] C.A. Charitidis, *Int. J. Refract. Met.* 28 (2010) 51.
- [27] T.F. Page, S.V. Hainsworth, *Surf. Coat. Technol.* 61 (1993) 201.
- [28] W. Dai, A. Wang, Q. Wang, *Surf. Coat. Technol.* 272 (2015) 33.
- [29] X. Yu, Z.W. Ning, M. Hua, C.B. Wang, *J. Adhes.* 89 (2013) 578.
- [30] J. Musil, *Surf. Coat. Technol.* 207 (2012) 50.
- [31] A. Leyland, A. Matthews, *Wear* 246 (2000) 1.